May 15, 1992

(100) surface segregation in Cu-Ni alloys

H.Y. Wang
R. Najafabadi
D. J. Srolovitz
Richard Alan Lesar, *Los Alamos National Laboratory*

PHYSICAL REVIEW B VOLUME 45, NUMBER 20 15 MAY 1992-II

(100) surface segregation in Cu-Ni alloys

H. Y. Wang, R. Najafabadi, and D. J. Srolovitz
Department of Materials Science and Engineering, University of Michigan, Ann Arbor, Michigan 48109

R. LeSar
Theoretical Division, Los Alamos National Laboratory, Los Alamos, New Mexico 87545
(Received 4 November 1991)

Atomistic simulations of segregation to the (100) free surface in Ni-Cu alloys have been performed for a wide range of temperatures and compositions within the solid-solution region of the alloy phase diagram. In addition to the surface-segregation profile, surface structures, free energies, enthalpies, and entropies were determined. These simulations were performed within the framework of the free-energy simulation method, in which an approximate free-energy functional is minimized with respect to atomic coordinates and atomic-site occupation. For all alloy bulk compositions ($0.05 \leq C \leq 0.95$) and temperatures ($400 \leq T \leq 1000$ K) examined, Cu segregates strongly to the surface and Ni segregates to the planes just below the surface. The width of the segregation profile is limited to approximately three atomic planes. The resultant segregation profiles are shown to be in good agreement with an empirical segregation theory. A simpler method for determining the equilibrium segregation in terms of the properties of unrelaxed pure Ni and pure Cu surface data is proposed and shown to be more accurate than the existing empirical segregation analyses. The surface thermodynamic properties depend sensitively on the magnitude of the surface segregation. The enthalpy, entropy of segregation, and the change in the interlayer spacing adjacent to the surface are shown to vary linearly with the magnitude of the surface segregation.

I. INTRODUCTION

Alloying elements and impurities often segregate to the surface or near-surface region of a solid. Since many material properties depend on surface properties, segregation plays an important role in such diverse phenomena as catalysis, thermionic emission, crystal growth, etc. Therefore, an understanding of these surface phenomena requires a knowledge of not only the structure of the surface, but also the surface composition. The surface composition, in turn, depends on the surface-segregation thermodynamics. The focus of the present work is the application of the recently introduced, free-energy simulation method to calculate the equilibrium structure, composition, and thermodynamics of surfaces in alloys. In particular, the present paper examines (100) surfaces in Cu-Ni alloys.

The observation that Cu segregates to surfaces in Cu-Ni alloys was suggested 20 years ago based upon measurements of catalytic activity, hydrogen adsorption, and work-function changes.[1–3] A trace amount of copper in the bulk was found to produce a large effect on the catalytic behavior of Ni, suggesting that copper strongly segregated to the surface. Experiments employing more modern surface analytical techniques followed in considerable numbers.[4–25] Although the experimental results differ somewhat in the degree of Cu enrichment and the concentration profile, most agree that the Cu concentration on the surfaces increases monotonically with increasing bulk Cu concentration. On the other hand, experiments by Sakurai *et al.*,[24] using the time-of-flight (TOF) atom probe, indicated that for bulk Cu concentrations greater than 84 at. %, Ni will segregate to the surface instead of Cu. These results have not been confirmed in other studies.

In addition to the experimental studies, there have been numerous theoretical investigations of the surface composition of Cu-Ni alloys. These studies have included Monte Carlo simulations[26–28] and electronic-structure-method-based investigations.[29–31] Almost all surface-segregation theories predict that Cu will segregate to the surface over the entire Ni-Cu phase diagram. However, one study, using tight-binding theory, did claim the existence of the reversal of surface segregant as the phase diagram is traversed.[32,33] They noted that if the condition of charge neutrality is imposed in the method used in Ref. 29, the crossover behavior will occur at 75 at. % bulk Cu concentration. Later, the same authors[29] investigated the effects of charge transfer on surface segregation and did not obtain the previously reported crossover.[30,31] They also pointed out that unphysical values of the difference between the Cu-Cu bond and Ni-Ni bond energy are necessary to produce the segregation reversal.

In addition to those described above, there are several theoretical methods for determining interfacial segregation, including lattice-gas models (regular solution), Monte Carlo methods, and tight-binding-type theory. The lattice-gas model is a simple model allowing for fairly straightforward theoretical analysis, but generally suffers from an unrealistic treatment of the interactions between the atoms. Some improved regular solution

models[20,34] do allow for limited relaxation of the interaction between the particles on the surface, but require an undetermined parameter to account for the degree of the relaxation. Tight-binding theory,[29–31] on the other hand, yields a very accurate description of the interaction between particles, but does not provide a simple method for determining the effects of temperature. Recent advances in Monte Carlo simulations[26–28] have extended these methods to alloy systems where the local composition may change during the course of the simulation. These methods may be employed to obtain accurate equilibrium segregation profile and interfacial structure provided that the interatomic potential which describes the interactions between atoms is accurate. Unfortunately, while this method does yield equilibrium interfacial structure and composition, it has never been successfully used to obtain interfacial free energies or other basic thermodynamic data. Monte Carlo calculations also require substantial computational resources and hence are generally limited to supercomputer applications and to studying relatively small numbers of interfaces and conditions.

The free-energy simulation method employed in the present study[35,36] is based on a number of simple approximations, centered on the concept of effective (or mean-field) atoms that have properties that are a concentration-weighted mix of those of the different atom types. The central approximations in the model are (1) the vibrations of the atoms are accounted for within the framework of the local harmonic (LH) model[37] in which the terms of the dynamical matrix that couple vibrations of different atoms are ignored; (2) a mean-field expression for the interaction energy described by embedded-atom-method (EAM) potentials is employed; and (3) the configurational entropy is calculated in the ideal-mixing limit. The most important feature of our method is that we develop a simple, approximate expression for the finite-temperature free energy of the system. Minimizing the free energy with respect to the positions and the mean composition of the atomic sites yields the equilibrium structure, segregation, and free energy, from which all other thermodynamic quantities may be derived.

This method is both physically and mathematically simple; yet its most crucial feature may be its computational efficiency. With this efficiency we are able to perform a large number of calculations to elucidate the trends in interfacial and segregation thermodynamics as a function of the experimental parameters, temperature, and bulk composition. In spite of its simplicity, however, this method is also very accurate. In Ref. 35, we reported preliminary results on segregation of Cu to $\Sigma 5$, $\Sigma 13$, and $\Sigma 61$ [001] twist grain boundaries and to (100), (110), and (111) free surfaces in the Cu-Ni system. We compared our prediction with segregation profiles determined from Monte Carlo (MC) simulations with the same potentials[26,27] and found close agreement. In most cases, our results were in quantitative agreement with the MC results and, in all cases, the qualitative trends were correct. Successes of the model included the accurate prediction of almost complete segregation of Cu segregation to, and Ni enhancement just below, Cu-Ni alloy surfaces. Thus, the model appears to be sufficiently accurate to predict the dominant physical features of surface segregation.

In the present paper, we report the results of a series of surface-segregation simulations in the Cu-Ni system. We performed simulation on (100) surfaces for a wide range of bulk concentrations ($0 \leq C_{\mathrm{Cu}} \leq 1$) and temperatures (400 K $\leq T \leq$ 1000 K), which includes the same physical parameter range as employed in our previous study of the Cu-Ni [001] twist boundaries.[36] We find that Cu is the dominant segregant in the Cu-Ni system at both the (100) free surface and the [001] twist grain boundary. However, Ni segregates to the second atomic plane from the free surface while Cu segregates to the second atomic plane from the grain boundary. The predicted surface- segregation profiles are analyzed in terms of existing segregation theory. The thermodynamic properties of the surface are shown to vary with the degree of segregation in a simple manner.

II. SIMULATION METHOD

In this section we outline the free-energy simulation method which we employ to determine the equilibrium structure, composition, and thermodynamics of defects in alloy systems. A more complete description is given elsewhere.[35,36] In the present approach, we construct an approximate free-energy functional for a multicomponent atomic system and then minimize it with respect to the atomic coordinates and the compositional profile in the material. The free energy of a multicomponent system consists of several distinguishable parts, including atomic bonding, atomic vibrations, and configurational entropy (i.e., the entropy associated with the relative spatial distribution of the atomic species). For metals, we describe the interactions within the framework of the embedded-atom-method (EAM).[39,40] The effects of atom vibrations are included within the framework of the local harmonic (LH) model,[37] which is given by

$$A_v = k_B T \sum_{i=1}^{N} \sum_{\beta=1}^{3} \ln \left[\frac{h \omega_{i\beta}}{2\pi k_B T} \right], \tag{1}$$

where A_v is the vibrational contribution to the free energy, $k_B T$ is the thermal energy, h is Planck's constant, N is the total number of atoms in the system, and ω_{i1}, ω_{i2}, and ω_{i3} are the three vibrational eigenfrequencies of atom i. These frequencies may be determined in terms of the local dynamical matrix of each atom $D_{i\alpha\beta} = \partial^2 E / \partial x_{i\alpha} \partial x_{i\beta}$, where E is the potential energy determined from summing the interatomic potential and the $x_{i\beta}$ correspond to atomic displacements of atom i in some coordinate system. Diagonalization of this 3×3 matrix yields the three force constants $k_{i\beta}$ for atom i. The vibrational frequencies are then determined as $\omega_{i\beta} = (k_{i\beta}/m)^{1/2}$, where m is the effective atomic mass. We have demonstrated that the approximations inherent in the LH model lead to errors in the free energy of perfect close-packed metal crystals of the order of 1% at the melting temperature and much less at lower temperatures.[37,38,41,42]

Configurational entropy is described on the basis of a point approximation, which is given as

$$S_c = -k_B \sum_{i=1}^{N} \{c_a(i)\ln[c_a(i)] + c_b(i)\ln[c_b(i)]\} , \quad (2)$$

where $c_a(i)$ is the concentration of a atoms and $c_b(i)$ is the concentration of b atoms on site i. Since we are interested in equilibrium properties, these concentrations may be viewed as the time-averaged composition of each atomic site in a system where the atoms are free to diffuse. In this sense, the atoms are "effective" or "mean-field" atoms. Since we replace real atoms by effective atoms, the internal energy E, which is defined in terms of the interatomic potential, must also be suitably averaged over the composition of each atom and its interacting neighbors. A method for performing these averages for the EAM potentials is described in Ref. 35 and 36.

The present simulations were performed within a reduced grand canonical ensemble, where the total number of atoms remains fixed but the relative quantities of each atomic species varies. The appropriate thermodynamic potential for this type of ensemble is the grand potential and is given by[43]

$$\Omega = A + \Delta\mu \sum_{i=1}^{N} c_a(i) = E + A_v - TS_c + \Delta\mu \sum_{i=1}^{N} c_a(i) , \quad (3)$$

where $\Delta\mu$ is the difference in chemical potential between the a and b atoms. In Eq. (3), A is the total Helmholtz free energy and E is the potential energy.

The equilibrium surface-segregation profile is determined in several steps. First, the properties of the perfect, uniform composition crystal are determined (see the Appendix). This is done by choosing a composition and then minimizing the Gibbs free energy, at the temperature and pressure of interest, with respect to the lattice parameter. Differentiating this equilibrium free energy with respect to composition gives the chemical-potential difference $\Delta\mu$. Since, at equilibrium, the chemical potential of a component is everywhere constant, we fix the chemical potential differences at their bulk values, introduce the appropriate surface, and minimize the grand potential with respect to the concentration and position of each atomic site.

The geometry of the cell used in the surface simulations is divided into two regions. The effective atoms in region I are completely free to move in response to the forces due to other atoms and the concentration at each site is allowed to vary. The atoms in region II, however, are constrained such that region II is a perfect crystal with the lattice constant and average concentration on each site appropriate to the simulation temperature, pressure, and bulk concentration. The equilibrium atomic configuration and the concentration of each effective atom are obtained by minimizing Eq. (3) with respect to the atomic coordinates and the site concentrations ($4N$ variables, where N is the number of atoms in the system). In the direction of the surface normal (i.e., the z direction) there are no constraints imposed on the particles, such that the traction in z direction is guaranteed zero. However, since periodic-boundary conditions are imposed in the x and y directions and the size of the surface in those directions is fixed by the lattice constant of the perfect system, some net stress may develop in the surface region. This is appropriate since the surface region in any but the thinnest films is constrained by the bulk crystal. The (100) surface, studied herein, was created simply by cleaving a single crystal along a (100) plane. The simulations were performed with a total of 20 atoms in each of the (002) planes included. Typically, eight (002) planes were required in order to obtain surface energies that were invariant with respect to increasing the number of planes in the simulation cell.

III. RESULTS

(100) Cu-Ni surface simulations were performed at four different temperatures: 400, 600, 800, and 1000 K. At each temperature, between 13 and 15 different bulk compositions were examined. In order to determine the equilibrium phases present at these temperatures and compositions, we mapped out the solid region of the Ni-Cu phase diagram. We find that above approximately 250 K, the solid is disordered. We have determined the melting points for pure Ni and Cu to be 1665 and 1290 K [38], respectively. These are in reasonable agreement with Monte Carlo simulation results using the same EAM potentials (i.e., Ni, 1740 K; and Cu, 1340 K) (Ref. 40) and experimental data (i.e., Ni, 1726 K; and Cu, 1358 K). Therefore, the temperatures and compositions examined in this study are well within the continuous solid-solution region of the phase diagram. The thermodynamic properties of the EAM Cu-Ni crystals over this temperature and composition range are reported in the Appendix.

The thermodynamic properties of the surfaces are distinguished from the bulk properties by the subscripts B or s, where B represents bulk (solid-solution) crystal properties and s refers to surface properties. The surface properties are defined as the difference between the property of the system containing the surface and that of a solid-solution crystal with the same number of atoms at the same bulk composition and temperature, $X_s = [X(\text{surface}) - X_B]/A$, where X is the thermodynamic property of interest (e.g., free energy, enthalphy, etc.) and the surface properties have been normalized by the surface area A. The surface properties may be calculated in two limits. The first is the unsegregated limit, as may be found by rapidly quenching the sample from very high temperature (where segregation is negligible) to the temperature of interest, and its properties are denoted by $X_{s,u}$. The second limit corresponds to equilibrium segregation at the temperature of interest and is denoted by $X_{s,s}$. The change in the thermodynamic properties that may be associated with the segregation is given by the difference between these two values, i.e., $\Delta X_s = X_{s,s} - X_{s,u}$.

Following segregation, the Cu concentration of the different (002) planes varies with layer number or distance from the free surface. The Cu concentrations on the (002) planes parallel to the surface are given by C_n, where the subscript n denotes the plane number (e.g., C_3 is the Cu concentration in the third (002) plane from the surface). We adopt the notation C_B as the dimensionless

bulk concentration far from the surface plane. Throughout this paper, all concentrations $0 \leq C \leq 1$ will refer to the Cu concentration; the Ni concentration is simply given by $1-C$. The degree of segregation, or *excess* concentration, is given by the difference between the concentration on a given atomic plane and the bulk concentration and is denoted $C_{n,xs}(=C_n - C_B)$. The net or *total excess* segregation is given by the sum of $C_{n,xs}$ over all (002) planes and is referred to as $C_{T,xs} = \sum_n C_{n,xs}$. Note, $C_{T,xs}$ is nonzero here, since in the present reduced grand canonical ensemble calculations the relative amounts of Cu and Ni are allowed to vary during the course of the simulation.

A. Segregation profiles

The concentration profile in the vicinity of the (100) surface is shown in Fig. 1 for different bulk concentrations C_B at $T=400$ K. Although the bulk concentration is varied from 20% to 80% Cu, the Cu concentration at the surface ($n=1$) remains approximately constant at 97% Cu (±2%). This corresponds to an excess Cu concentration at the first plane of 76% for $C_B=0.2$ and 19% for $C_B=0.8$. Unlike in the Σ5 [001] twist grain boundary,[36] the second (002) plane from the surface ($n=2$) exhibits Ni segregation, although to a smaller degree than the first (002) plane. The third (002) plane also shows Ni segregation with an even smaller magnitude. By the fourth (002) plane from the surface, the Cu concentration is nearly equal to the bulk concentration. These segregation profiles indicate that the effective width of the free surface-segregation profile is approximately three (002) planes and that the total excess concentration $C_{T,xs}$ for

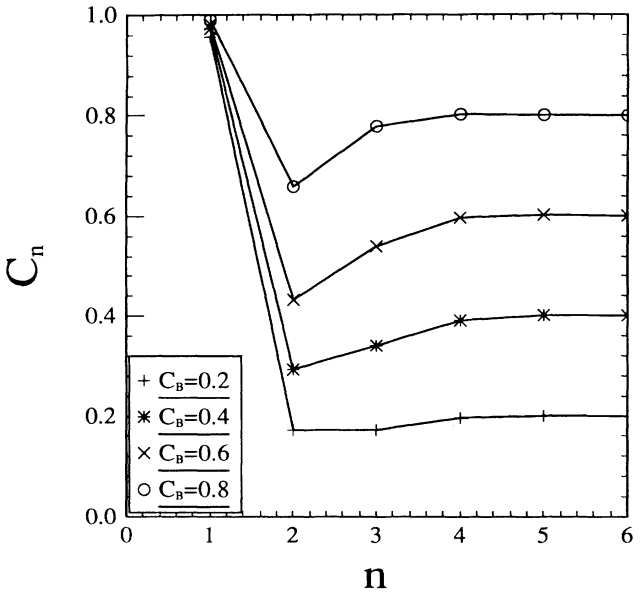

FIG. 1. Concentration of Cu atoms on (002) planes parallel to the surface vs layer number n, where $n=1$ corresponds to the (002) plane adjacent to the surface. The temperature is 400 K and the plus, asterisk, cross, and circle are for bulk concentrations of 0.2, 0.4, 0.6, and 0.8, respectively.

C_B less than about 0.5 is dominated by $C_{1,xs}$. When C_B is bigger than 0.5, however, the contribution from the second layer is quite significant.

The bulk concentration dependence of the segregation on the different planes may be seen more clearly in Fig. 2(a), where the concentration on the first four (002) planes are plotted as a function of the bulk concentration at 400 K. In this type of plot, the straight line $C_n=C_B$ corresponds to zero segregation. Clearly, C_n must go to zero as C_B approaches zero and C_n must go to one as C_B approaches 1 since in these limits no solute is present. In toto, these curves show that the first plane has Cu segregation, the second and the third planes have Ni segregation as we have seen in Fig. 1. The fourth plane, however, shows very little segregation; when $C_B > 0.7$ there is slight Cu segregation and when $C_B < 0.7$ Ni weakly segregates. The effects of temperature and bulk concentration on the first layer segregation is shown in Fig. 2(b), where we plot C_1 as a function of the bulk concentration for four temperatures. This curve shows that Cu always segregates to the surface, but to a lesser degree with increasing temperature.

The relationship between the segregation to the surface ($n=1$) and the total segregation may be seen more clearly in Fig. 2(c), where we plot $C_{1,xs}=C_1-C_B$ (solid line) and $C_{T,xs}$ (dash-dot-dot line) vs C_B for four different temperatures. The maximum degree of segregation always occurs at $C_B < 0.5$ and shifts to lower C_B with decreasing temperature. In all cases, the net or total segregation is less than that to the $n=1$ (002) plane, due to the predominance of Ni segregation for $n \geq 2$. As the temperature is decreased and/or the bulk concentration is increased, the large segregation of Ni to the second layer yields a significant difference between $C_{T,xs}$ and $C_{1,xs}$. Nonetheless, at the higher temperatures, $C_{1,xs}$ is still a reasonably good approximation to $C_{T,xs}$, indicating the sharpness of the segregation profile. As the temperature is increased from 400 to 1000 K, both $C_{T,xs}$ and $C_{1,xs}$ decrease.

Taken together, the segregation-profile data for the (100) surface in the Cu-Ni system can be summarized as follows: (1) there is a net segregation of Cu to the surface for all bulk concentrations and temperatures, (2) the segregation profile is effectively limited to the three (002) atomic planes near the surface, (3) Ni segregates to the $n \geq 2$ planes with a smaller magnitude than the first-layer Cu segregation, and (4) the total amount of segregation, the segregation to the first layer, and the difference between these quantities decrease with increasing temperature.

B. Thermodynamics

All of the surface thermodynamic properties are defined as the difference between those properties in the system with the surface and that of the bulk (see the Appendix) and normalized by the area of the surface, as described above. The surface free energy, in the grand canonical ensemble, is denoted as $\Gamma_s=(\Omega_s-\Omega)/A$, where Ω_s is the grand potential of the system with the surface, Ω is the grand potential for the perfect crystal,

and A is the area of the surface. Γ_s is plotted as a function of bulk concentration C_B in Fig. 3 both with (solid curves) and without (dotted curves) segregation. For the calculations with segregation, the grand potential is minimized with respect to the position and the concentration of each site, while for the unsegregated surface, the compositions of each site are fixed at C_B and the grand potential is minimized only with respect to the atomic coordinates. The bulk concentration dependence of the unsegregated surface grand potential is quite simple; the $\Gamma_{s,u}$ vs C_B curves are approximately linear interpolations between the pure Ni and the pure Cu Γ_s values and the effect of increasing temperature is simply to shift these curves to lower values of Γ_s. This temperature dependence is primarily a consequence of the positive surface entropy,[42] as discussed below

The Γ_s vs C_B curves for the segregated surfaces are much more complicated than in the unsegregated case. The complexity is introduced by the competition between the various terms that make up the free energy: enthalpy, entropy, and chemical potential. The lower the temperature, the smaller the entropic contribution to the free energy, such that $\Gamma_{s,s}$ is larger. However, since segregation is more pronounced at lower temperatures, the larger the contribution from the energy that drives segregation (this is $H-\Delta\mu\, C_{T,xs}$), and, hence, the smaller the magnitude of $\Gamma_{s,s}$. For bulk Cu concentrations less than approximately 0.5, $\Gamma_{s,s}$ is smallest for the lowest temperature studied

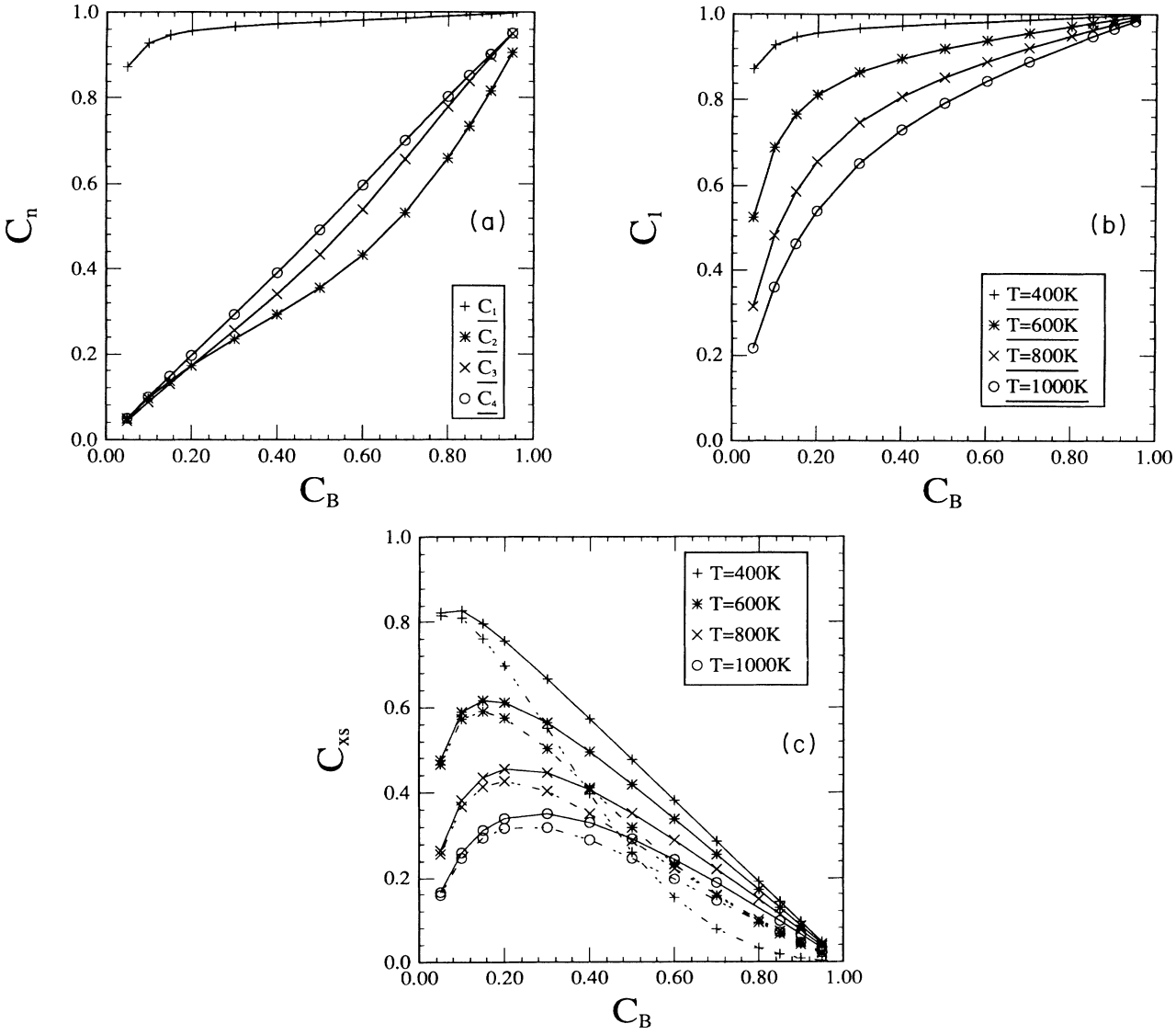

FIG. 2. The Cu concentration of the first four (002) planes C_1 (plus), C_2 (asterisk), C_3 (cross), and C_4 (circle) are plotted as functions of the bulk concentration C_B at $T=400$ K (a). The Cu concentration on the first layer C_1 (b) and the excess concentrations (c) are plotted as functions of the bulk concentration C_B. The plus, asterisk, cross, and circle are for 400, 600, 800, and 1000 K, respectively. In (c), the solid lines correspond to the first-layer excess concentration $C_{1,xs}$, and the dashed lines to the total excess concentration $C_{T,xs}$.

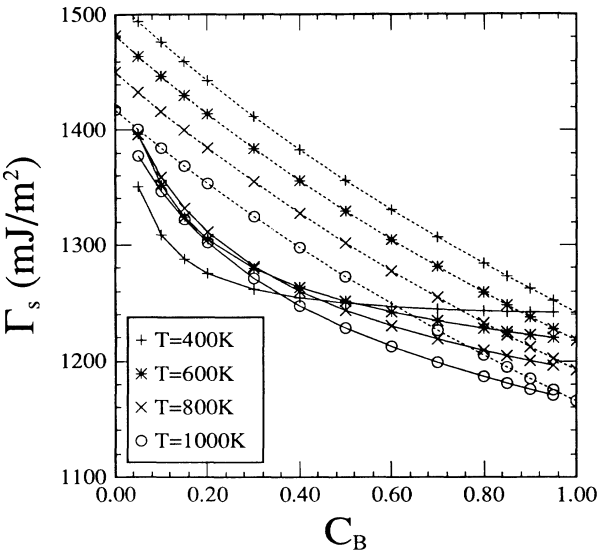

FIG. 3. The surface grand potential vs the bulk concentration. The solid lines are for the segregated surface, while the dashed lines are for the unsegregated surface. The plus, asterisk, cross, and circle are for 400, 600, 800, and 1000 K, respectively.

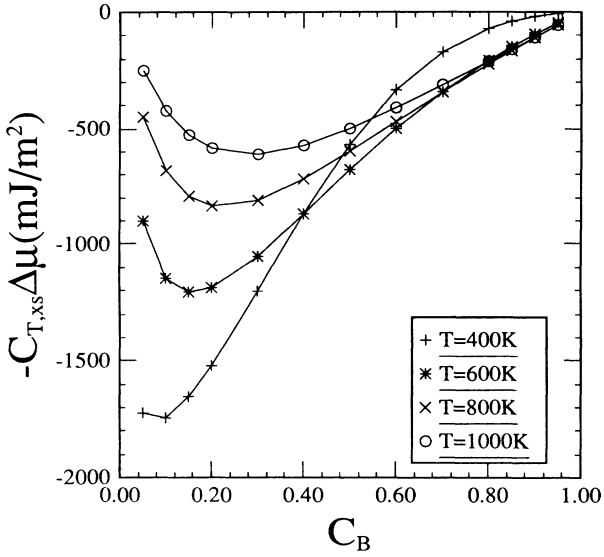

FIG. 4. The chemical-potential contribution to the grand potential $-C_{T,xs}\,\Delta\mu$ vs the bulk concentration. The plus, asterisk, cross, and circle are for 400, 600, 800, and 1000 K, respectively.

($T=400$ K). For $C_B>0.5$, the smallest surface free energy is found at the highest temperature studied ($T=1000$ K). These results may be understood by considering the effects of bulk concentration and temperature on the segregation behavior [see Fig. 2(c)]. The degree of Cu segregation is greatest at low temperatures and for bulk concentrations on the Ni-rich side of the phase diagram. In this regime (low T, small C_B), where the degree of segregation is a maximum, $\Gamma_{s,s}$ is a minimum. On the other hand, at high T and large C_B the degree of segregation is small. In this regime, the ordering of the different temperature curves in the $\Gamma_{s,s}$ vs C_B plot are as they are in the absence of segregation.

In order to understand $\Gamma_{s,s}$, we can examine the terms that contribute to it independently: the enthalpy H_s, the entropic term TS_s, and the chemical-potential term $C_{T,xs}\,\Delta\mu$. In Fig. 4, $-C_{T,xs}\,\Delta\mu$, the contribution of the chemical potential to $\Gamma_{s,s}$, is plotted against the bulk concentration, where $\Delta\mu$ (see Fig. 13) is the chemical-potential difference between Cu and Ni and $C_{T,xs}$ [see Fig. 2(c)] is the total excess concentration of Cu. This term is zero for pure Cu and for pure Ni, since $C_{T,xs}$ is zero there, and has a minimum at $0.15<C_B<0.35$. The position of the minimum moves to smaller C_B with decreasing temperature. For the range of concentrations and temperatures shown in Fig. 4, $\Delta\mu$ is positive and is of order unity (see the Appendix). That $-C_{T,xs}\,\Delta\mu$ is negative indicates that the chemical-potential contribution favors Cu segregation.

S_s is defined as minus the partial derivation of the surface grand potential Γ_s with respect to temperature at fixed pressure and chemical potential. Alternatively, S_s may be defined as minus the partial derivative of the surface free energy G_s with respect to temperature at fixed pressure and composition. $S_{s,u}$ was determined from the G_s data in this manner. The dependence of the surface entropy S_s on the bulk concentration C_B is plotted in Fig. 5(a) for four different temperatures, with and without segregation. $S_{s,u}$ varies only slightly with composition and temperature in this alloy system; decreasing smoothly from its pure Ni to its pure Cu value.

The same numerical method for calculating $S_{s,u}$ cannot be applied to the determination of $S_{s,s}$ since we have neither a series of Γ_s data at constant chemical potential (at fixed C_B, $\Delta\mu$ varies with T) nor a series of G_s data at constant *surface* composition. The method we employed to determine $S_{s,s}$ was to equilibrate the surface at a particular temperature T, determine its free energy $G(T)$, and then evaluate $G(T+\Delta T)$ and $G(T-\Delta T)$ with the same surface structure and composition profile equilibrated at temperature T. $S_{s,s}$ at T was then determined from $S_{s,s}=-[G(T+\Delta T)-G(T-\Delta T)]/2\Delta T$. This method is clearly approximate; however, since the free energy can be determined rapidly at any temperature for fixed structure and composition profile, it is very efficient. In order to determine the accuracy of the method, we determined $G(T+\Delta T)$ and $G(T-\Delta T)$ from full relaxations at $T+\Delta T$ and $T-\Delta T$ for a few cases in the grain boundary calculations.[36] We find that if we limit ΔT to be less than 10 K, the values of the entropy determined using the fully relaxed and approximate methods differed by less than 0.01%. The surface entropy in the segregated case [Fig. 5(a)] has a well-defined maximum at $C_B<0.2$ and a well-defined minimum at $C_B\geq 0.8$. Both the low C_B maximum and the high C_B minimum become more pronounced with decreasing temperature. This relatively complex behavior may be traced to the fact that the $S_{s,s}$

has two physically different components: configurational and vibrational.

The surface configurational entropy $S_{s,c}$, determined from Eq. (2), is plotted as a function of the bulk concentration C_B in Fig. 5(b). Like S_s itself, $S_{s,c}$ has both low C_B maxima and high C_B minima which become more pronounced with decreasing temperature (i.e., increasing segregation). $S_{s,c}$ must go to zero at both $C_B=0$ and $C_B=1$, since there is no segregation in pure systems. The maxima in $S_{s,c}$ occurs at small C_B where segregation is most severe and the minima occur at higher C_B, where segregation is weak. The values for $S_{s,c}$ are negative at the minimum because the configurational entropy of the bulk is a maximum at $C_B=0.5$ and $S_{s,c}$ is the difference between the configurational entropy of the system with and without the surface. In fact, the shape of the $S_{s,c}$ versus composition curve can be reasonably well reproduced from the composition dependence of the perfect-crystal configurational entropy by replacing C_B on the abscissa of Fig. 15(b) with C_1 and subtracting the original perfect-crystal configurational entropy.

The surface vibrational entropy, including both harmonic and anharmonic contributions, may be determined as $S_{s,v}=S_s-S_{s,c}$ and is plotted as a function of the bulk concentration in Fig. 5(c). The unsegregated-surface vibrational entropy (dotted curves) is equal to the total surface entropy, since $S_{s,c}$ is zero for the unsegregated surface. The segregated-surface vibrational entropy (solid curves) is reminiscent of the dependence of the excess surface concentration $C_{T,xs}$ on C_B [see Fig. 2(c)]. The segregated-surface vibrational entropy exhibits a maximum at approximately the same C_B as the maximum in

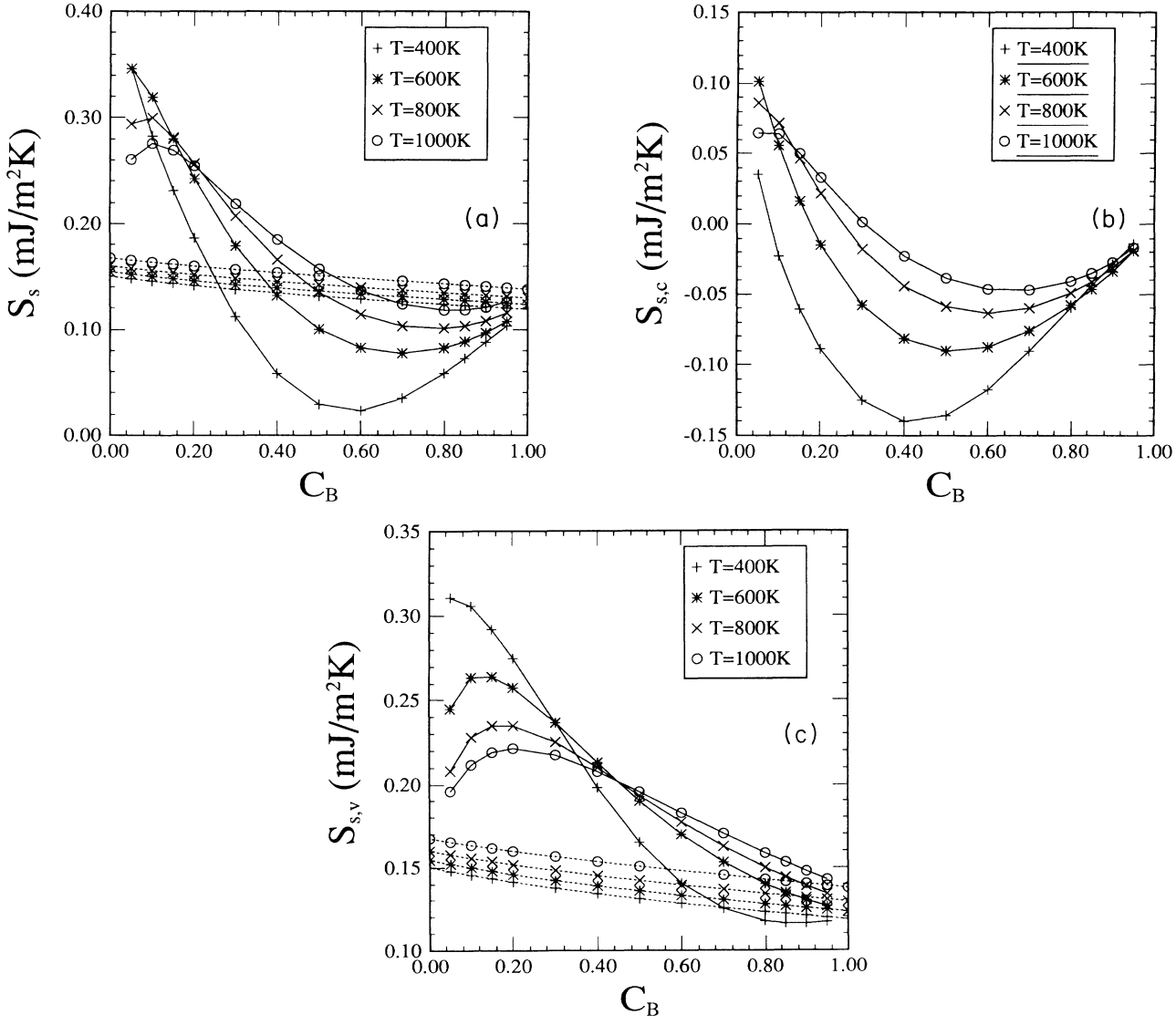

FIG. 5. (a) The total surface entropy, (b) configurational entropy, (c) and vibrational entropy vs the bulk concentration. The solid lines are for the segregated surface, while the dashed lines are for the unsegregated surface. The plus, asterisk, cross, and circle are for 400, 600, 800, and 1000 K, respectively.

the excess concentration, which may be understood in terms of the relative magnitude of the vibrational entropy of pure Ni and pure Cu. Figure 15(a) clearly shows that the vibrational entropy of Ni is lower than that of Cu and that the vibrational entropy of the solid solution alloy is nearly a linear interpolation between these limits (Vegard's law). Therefore, the form of the $S_{s,v}$ vs C_B plot is directly attributable to the degree of segregation present and the linear form of the composition dependence of the vibrational entropy.

The surface enthalpy may be determined from knowledge of the surface free energy and the other thermodynamic data: $H_s = \Gamma_s + C_{T,xs}\,\Delta\mu + TS_s$. The dependence of H_s on the bulk concentration is shown in Fig. 6. Again, the enthalpy of the unsegregated surface (dotted) is very simple, decreasing from the pure Ni to the pure Cu value in a nearly linear manner. Furthermore, the enthalpy of the unsegregated surface is only weakly temperature dependent. In the case of the segregated surface (solid), the dependence of the surface enthalpy on temperature is again reminiscent of the bulk concentration dependence of the excess surface concentration $C_{T,xs}$. $H_{s,s}$ has a well-defined maximum at small C_B and increases with decreasing temperature. As with the vibrational entropy, the enthalpy of the perfect crystal exhibits a nearly linear increase with Cu concentration from a small value in pure Ni to a larger value in pure Cu (see Fig. 14). Therefore the form of the $H_{s,s}$ plot in Fig. 6 may be attributed to the bulk concentration dependence of the Cu segregation and the proportionality between Cu concentration and the enthalpy. Since $H_{s,s} - H_{s,u} > 0$, enthalpy discourages segregation (i.e., raises Γ_s). It is, in fact, $H_s - \Delta\mu\, C_{T,xs}$ that favors segregation (compare Figs. 4 and 6).

The freedom of particles to move in the direction normal to the surface results in zero net surface traction. Associated with these atomic motions is a change in the separation between the (002) planes near the surface. The *change* of the separation between the nth and the $(n+1)$th planes, $d_{n,n+1}$, is defined as the difference between the separation of those two planes in a solid with and without a surface. The bulk concentration dependence of $d_{1,2}$, $d_{2,3}$, and $d_{3,4}$ is plotted in Figs. 7(a)–7(c), respectively. In the unsegregated cases (dotted line), $d_{1,2}$ decreases from the value in pure Ni to that in pure Cu with very little curvature. Except for $T=400$ K, where $d_{1,2}$ for an unsegregated surface is negative over the whole bulk concentration region, $d_{1,2}$ is positive at the Ni-rich end and negative at the Cu-rich end of the phase diagram. While calculations at $T=0$ for both pure Ni and Cu using the present EAM potentials[40] yield negative $d_{1,2}$, the common observations of inward surface relaxations may not generally hold at elevated temperatures. For the segregated surfaces (solid line), the value of $d_{1,2}$ is generally larger than that of the corresponding unsegregated case, due to the strong first-layer Cu segregation and the fact that Cu atoms are larger than Ni atoms. The exception to this trend is in the region of $C_B > 0.7$ and $T=400$ K, which may be the result of the strong Ni segregation to the second layer. For $d_{2,3}$ and $d_{3,4}$, the unsegregated curves (dotted line) are simply linear interpolations between the value for pure Ni and pure Cu. $d_{2,3}$ for the segregated surface is always smaller than in the unsegregated case, due to the Ni segregation to the second and the third plane. $d_{3,4}$ is smaller with segregation than without for $C_B < 0.8$ and larger for $C_B > 0.8$, which may be the result of Ni segregation to the fourth layer for $C_B < 0.7$ and weak Cu segregation for $C_B > 0.7$.

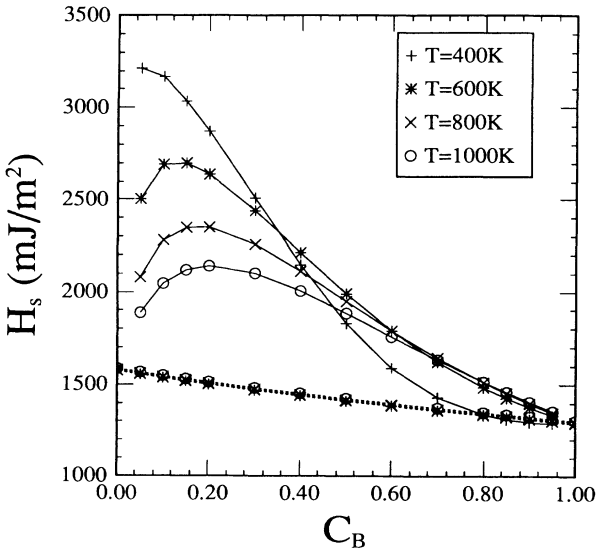

FIG. 6. The surface enthalpy H_s vs the bulk concentration. The solid lines are for the segregated surface, while the dashed lines are for the unsegregated surface. The plus, asterisk, cross, and circle are for 400, 600, 800, and 1000 K, respectively.

IV. DISCUSSION

Comparison of the simulation results on the segregated and unsegregated surfaces demonstrates that the degree of segregation plays a major role in determining the surface thermodynamics. For the unsegregated surface, the surface properties (such as the free energy, entropy, enthalpy, and expansion) vary with concentration in a very simple, smooth manner and variations with temperature simply result in nearly uniform shifts of the property-versus-composition curves. The segregated surface, on the other hand, shows very complicated behavior, which can be understood by examining the different contributions to the free energy.

To investigate the nature of the correlations between segregation and surface properties, we need to focus on the thermodynamic properties that depend on the segregation and not on the intrinsic properties of the surface itself, i.e., the excess thermodynamic properties defined earlier, i.e., $\Delta X_s = X_{s,s} - X_{s,u}$, where X is the property of interest. Figure 8(a) shows the excess vibrational entropy $\Delta S_{s,v}$ as a function of the total excess concentration $C_{T,xs}$. Similarly, Figs. 8(b) and 8(c) show the excess enthalpy ΔH_s and the excess separation between the first two planes $\Delta d_{1,2}$ as a function of $C_{T,xs}$. These plots con-

sist of data taken over the entire range of temperature and concentration reported in the previous section. In all three cases, we find that there is a linear relationship between these surface thermodynamic properties and the total excess concentration. Linear numerical fits to this data yield $\Delta X_s = mC_{T,xs}$ with the slope $m = 0.190 \pm 0.002$ mJ/m^{2}K for $\Delta S_{s,v}$, 1956 ± 14 mJ/m^2 for ΔH_s, and 0.0367 ± 0.0004 Å for $\Delta d_{1,2}$. The configurational contribution to the excess surface entropy $\Delta S_{s,c}$ does not exhibit a linear dependence on $C_{T,xs}$ due to the explicitly prescribed nature of the configurational entropy [Eq. (2)]. The excess surface grand potential $\Delta\Gamma_s$ is approximately a linear function of $C_{T,xs}$. However, due to the presence of the $\Delta S_{s,c}$ term, there is considerably more scatter than for $\Delta S_{s,v}$, ΔH_s, and $\Delta d_{1,2}$.

We have previously calculated the thermodynamic properties for a grain boundary in Cu-Ni binary alloys as a function of temperature and bulk concentration,[36] where we considered the cases with and without segregation. For the case where no segregation is allowed, the thermodynamic properties of the grain boundaries (e.g., free energy, entropy, enthalpy, and the separation between planes at the boundaries) show almost the same scaling with bulk concentration and the temperature as we find here for the free surface. However, the overall segregation is different in detail for the two types of interfaces. First, the width of the boundary in terms of the segregation profile is somewhat larger for the free surface than for the grain boundary. We found the boundary width for the grain boundary studied[36] to be approxi-

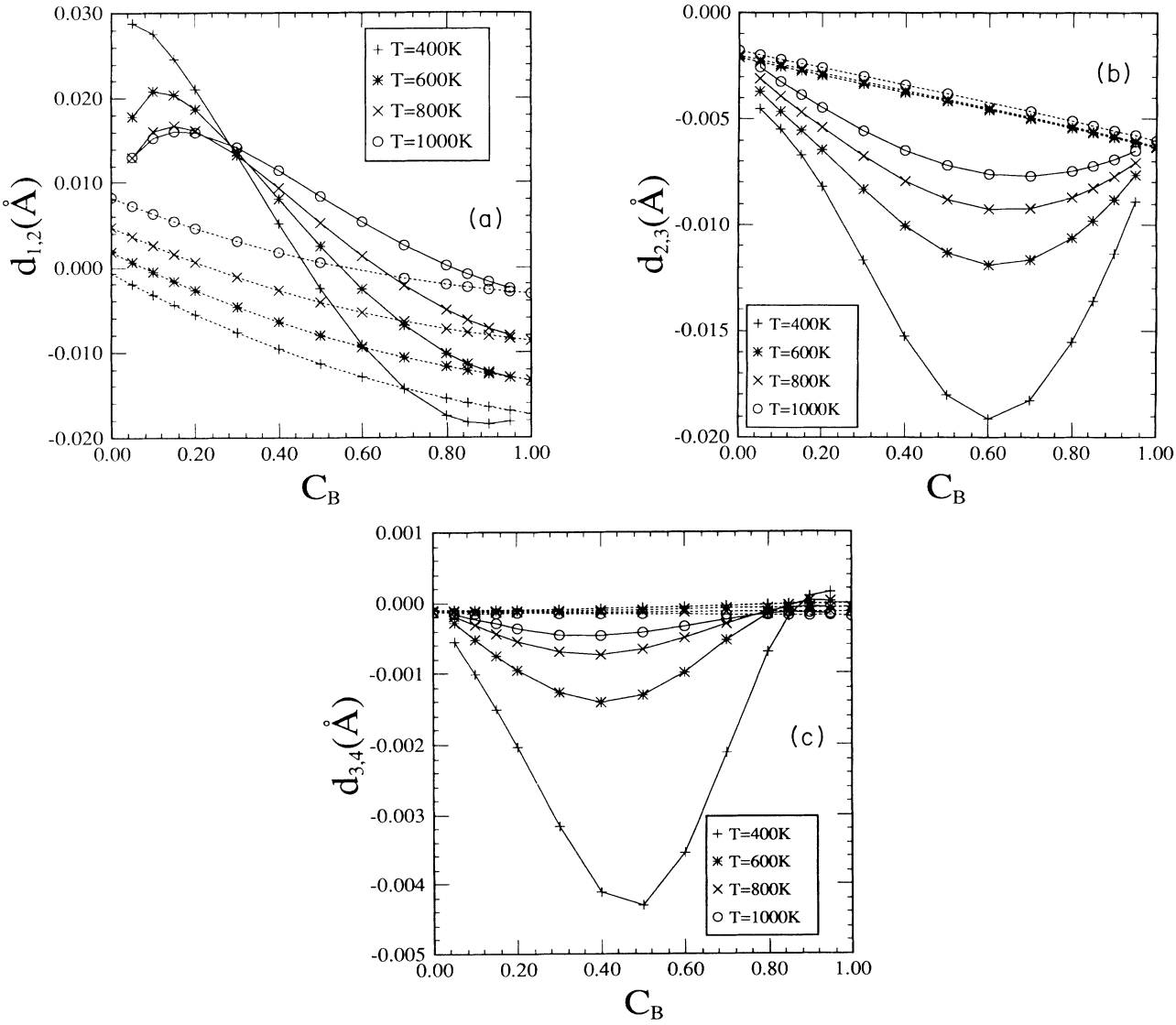

FIG. 7. The change of the separation between the first three pairs of planes (a) $d_{1,2}$, (b) $d_{2,3}$, and (c) $d_{3,4}$ vs the bulk concentration. The change of the separation between a pair of planes is defined as the difference between the spacing between two atomic planes and their separation in a perfect crystal. The solid lines are for the segregated surface, while the dashed lines are for the unsegregated surface. The plus, asterisk, cross, and circle are for 400, 600, 800, 1000 K, respectively.

mately two layers on each side of the interface. For the surface studied here, however, the segregation decays somewhat slower, with a width of three layers instead of two. Cu segregates strongly to both grain boundary and free surface, although the grain-boundary segregation was found to be weaker than the surface segregation. However the total excess concentration is quite different, due to the tendency for Ni segregation in the second (002) layer from the surface and the Cu segregation to the second (002) layer from the grain boundary. As in the free-surface case, most of the grain-boundary excess thermodynamic properties exhibit a linear dependence on the total excess concentration.

As described above, all of the equilibrium surfaces were obtained by minimizing the ground potential Ω [Eq. (3)] with respect to the position and the concentration of each site in the system. Taking the derivative of the minimized grand potential Ω with respect to the concentration of plane n thus yields an analytic formula for calculating the concentration on plane n,[44]

$$\frac{C_n}{1-C_n}=\frac{C_B}{1-C_B}\exp\left[-\beta\left[\frac{\partial F}{\partial C_n}-\frac{\partial F}{\partial C_B}\right]\right], \tag{4}$$

where $\beta=1/k_BT$ and F is the free energy of the system excluding the configurational entropy

$$F=E+A_v\ . \tag{5}$$

Classical theories of segregation, such as Langmuir-McLean and Fowler-Guggenheim models, are based on approximations to the heat of segregation

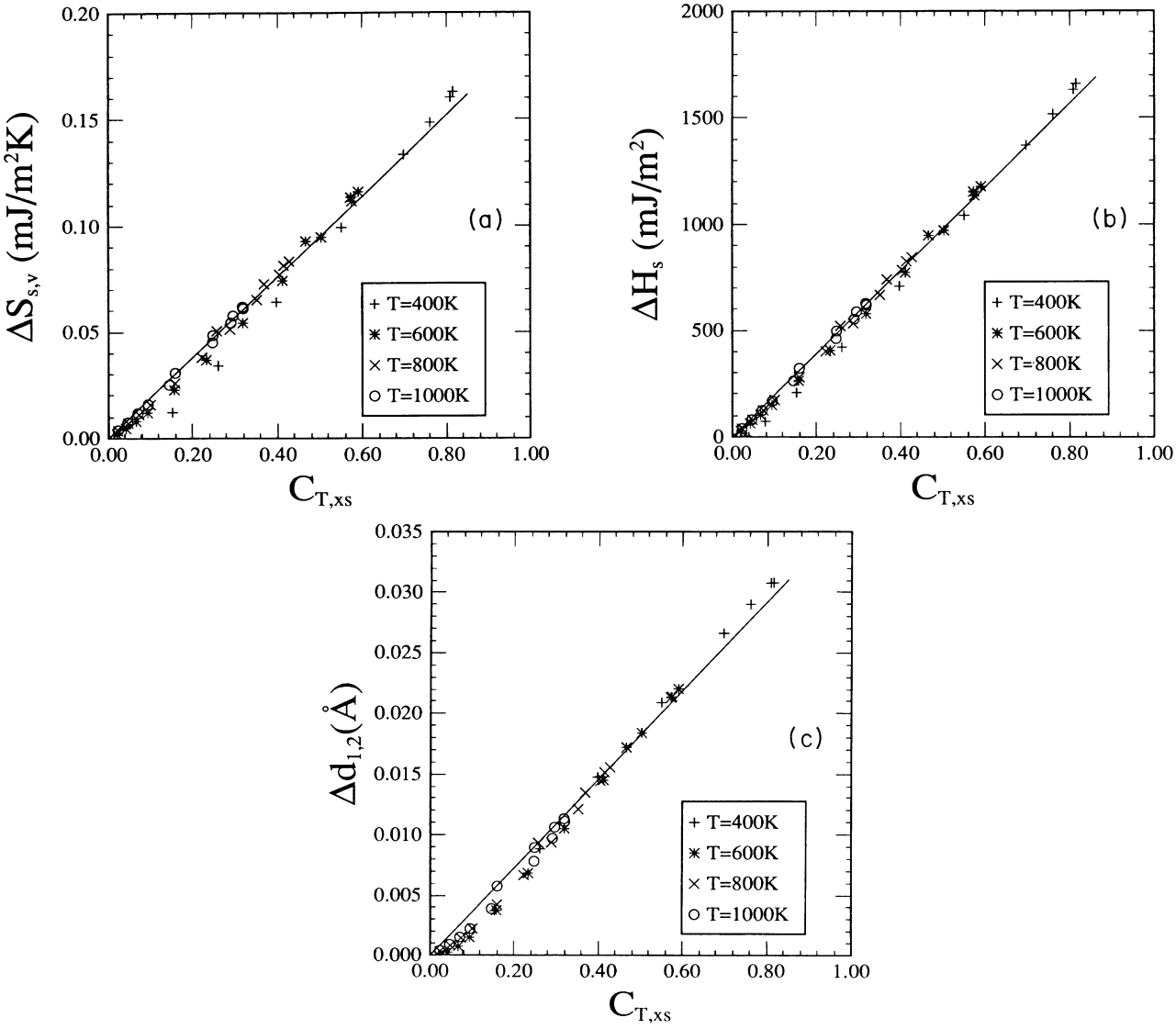

FIG 8. (a) The excess surface vibrational entropy ΔS_s, (b) excess surface enthalpy ΔH_s, and (c) excess separation between the first two (002) planes $\Delta d_{1,2}$ vs the total excess concentration. All of these quantities are simply the difference between their values with and without segregation. The plus, asterisk, cross, and circle are for 400, 600, 800, and 1000 K, respectively. The straight lines are fit to all of the data in each figure.

$Q_n(=\partial F/\partial C_n-\partial F/\partial C_B)$. The Langmuir-McLean formula is derived on the basis of first-layer segregation, with noninteracting segregants and equivalent segregation sites, i.e., the heat of segregation Q_1 is a *constant*. The Fowler and Guggenheim model[45] is somewhat more sophisticated in that nearest-neighbor interactions are included, and Q_1 is thus a linear function of the surface concentration,

$$Q_1=\alpha C_1+\Delta G\ , \tag{6}$$

where α is a constant that is determined by the coordination number of the segregant sites and the strength of the interaction between solutes.

Our results for Q_1 (evaluated as $\partial F/\partial C_1-\partial F/\partial C_B$) are plotted as a function of the bulk concentration C_B in Fig. 9. It is clear that Q_1 is neither a constant nor simply a linear function of the surface concentration, but is much closer to a linear function of the bulk concentration. It is not surprising then that the Langmuir-McLean formula and the Fowler-Guggenheim model are not good approximations to the surface segregation found in the present study.

A later model[20,34] modified the Fowler-Guggenheim method to include interactions within the surface layer and the bulk and also included a parameter δ which empirically accounts for surface relaxation. In this model, the heat of surface segregation Q_1 is given as

$$Q_1=\left[\Delta H_{\rm sub}\frac{[Z_v-(Z_1+Z_v)\delta]}{Z}+2\Omega\left[ZC_B-(1+\delta)Z_1C_1-(1+\delta)Z_vC_B+\frac{\delta}{2}Z_1+\frac{\delta-1}{2}Z_v\right]\right]\ , \tag{7}$$

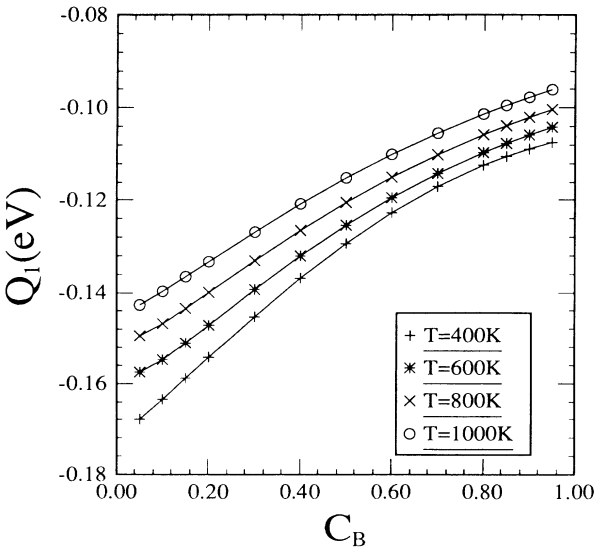

FIG. 9. The heat of surface segregation Q_1 $(=\partial F/\partial C_1-\partial F/\partial C_B)$ for the relaxed surface vs the bulk concentration C_B. The plus, asterisk, cross, and circle are for 400, 600, 800, and 1000 K, respectively.

where $\Delta H_{\rm sub}$ is related to the difference of the sublimation energy between A and B atoms; Ω is the regular solution parameter defined as $\varepsilon_{AB}-0.5(\varepsilon_{AA}+\varepsilon_{BB})$, and ε_{AB}, ε_{AA}, and ε_{BB} are the interaction energies between A-B, A-A, and B-B bonds, respectively; Z_1, Z_v, and Z are the number of lateral surface bonds, vertical surface bonds, and perfect-crystal nearest-neighbors bonds, respectively. Within the framework of this model, the value of $\Delta H_{\rm sub}$ is estimated by relating the sublimation energy and the surface energy. For the (100) surface, the sublimation energy of the pure material $H_{\rm sub}$ is given by

$$H_{\rm sub}=\frac{Z\gamma\sigma}{Z_v}=3\gamma\sigma \tag{8}$$

based upon a simple bond-counting argument, where γ is the surface energy and σ is the area per atom. However, this result is known empirically[46] to underestimate $H_{\rm sub}$ by about a factor of 2, thus we use $H_{\rm sub}=6\gamma\sigma$ and the difference of the sublimation energy between A atom and B atom is given by

$$\Delta H_{\rm sub}=6(\gamma_A\sigma_A-\gamma_B\sigma_B)\ . \tag{9}$$

The regular solution parameter is evaluated by replacing one atom of the perfect crystal A with a B atom and then calculating the difference of the energy between these two crystals. If the atoms interact with nearest-neighbor pair interactions, that difference is roughly equal to $12(\varepsilon_{AB}-\varepsilon_{AA})$. Similarly, by replacing one atom of the perfect crystal B with an A atom, we will have the difference of $12(\varepsilon_{AB}-\varepsilon_{BB})$. The addition of these two differences divided by 24 is the value of Ω. Using this approach with the EAM potentials employed in the present study we find $\Delta H_{\rm sub}=0.495$ eV/atom and $\Omega=0.0042$ eV. In order to apply this method of determining the equilibrium surface segregation, we need to determine the value of the parameter δ in Eq. (7). Best fit to our surface-segregation data as a function of bulk concentration and temperature was obtained with $\delta=0.16$. Figure 10 shows C_1 versus the bulk concentration results obtained for our simulation along with the behavior predicted by Eq. (7) with all of the parameters chosen as above. In general, the agreement found between simulation and the empirical δ formalism is excellent over the entire range of data. The theoretical predictions slightly overestimate the magnitude of the Cu surface segregation on the Ni side of the phase diagram and underestimate it on the Cu rich side.

If δ is set to zero, then Eq. (7) is closely related to the Fowler-Guggenheim model, which does not fit the segregation results from the simulations. The parameter δ is introduced in the model to account for the relaxation of the surface. However, since δ was obtained by fitting to the simulation data, it probably accounts for other inaccuracies in the theory. These may include interactions beyond nearest neighbors, many-body effects, vibrational entropy, segregation to atomic planes below the surface, etc.

In order to examine the effect of surface relaxations on surface segregation we compare the heat of segregation Q_1 with and without relaxation based upon our 400 K

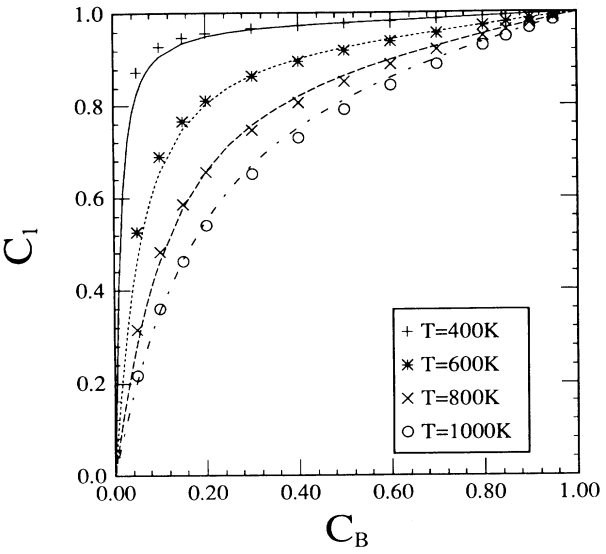

FIG. 10. The Cu concentration on the first layer C_1 given by the simulation (symbols) and by Eq. (7) (lines) vs the bulk concentration C_B. The plus and solid line, asterisk and dotted line, cross and dashed line, and the circle and dashed-dotted line are for 400, 600, 800, and 1000 K, respectively.

simulation data in Fig. 11(a). This figure shows that the heat of segregation for the relaxed and unrelaxed surfaces are nearly identical. Therefore, contrary to the above results, surface relaxation plays only a very minor role in surface segregation on the (100) surface of Cu-Ni alloys.

Figure 11(a) also demonstrates that the variation of the heat of segregation from pure Cu to pure Ni is relatively smooth and slowly varying. Therefore, we will attempt to model surface segregation in this system via a linear interpolation of the Q_1 values between the pure Ni and pure Cu limits. To further simplify the present analysis, we will employ only the pure Ni and pure Cu values of Q_1 taken from the simulation without relaxation. A comparison between the equilibrium segregation data at a variety of bulk compositions and temperatures and predictions based upon the linear interpolation of the unrelaxed Ni and Cu data is shown in Fig. 11(b). The excellent fit between this very simple approximation and the full simulation data is of even better quality than obtained from the δ formalism of Eqs. (7)–(9). This simple linear interpolation may be made even easier by performing the analysis at $T=0$ K. This further simplification is based upon the observation that the change in the vibrational contribution to Q_1 is essentially negligible as long as the proper temperature-dependent lattice constant is employed. Thus, if we estimate the values of $Q_1=\partial E/\partial C_1-\partial E/\partial C_B$ for pure Ni and pure Cu at $T=0$ K without using any relaxations, then the surface concentration can be easily (and accurately) estimated with little work. We are currently investigating the generality of this method for a wide range of alloy systems.

The EAM potentials used in the present study were developed by Foiles, Baskes, and Daw.[40] These interatomic potentials were designed to consistently describe the metals Cu, Ni, Ag, Au, Pd, and Pt and their alloys. Foiles[26] developed another set of EAM potentials specifically for the Cu-Ni system. The details of the surface segregation results found with the two EAM potentials are significantly different.[47] The segregation results calculated with these special Cu-Ni potentials[26] are somewhat closer to the experimental values. However, the potential given by Foiles, Baskes, and Daw[40] is sufficiently accurate for the purpose of the present paper, which are

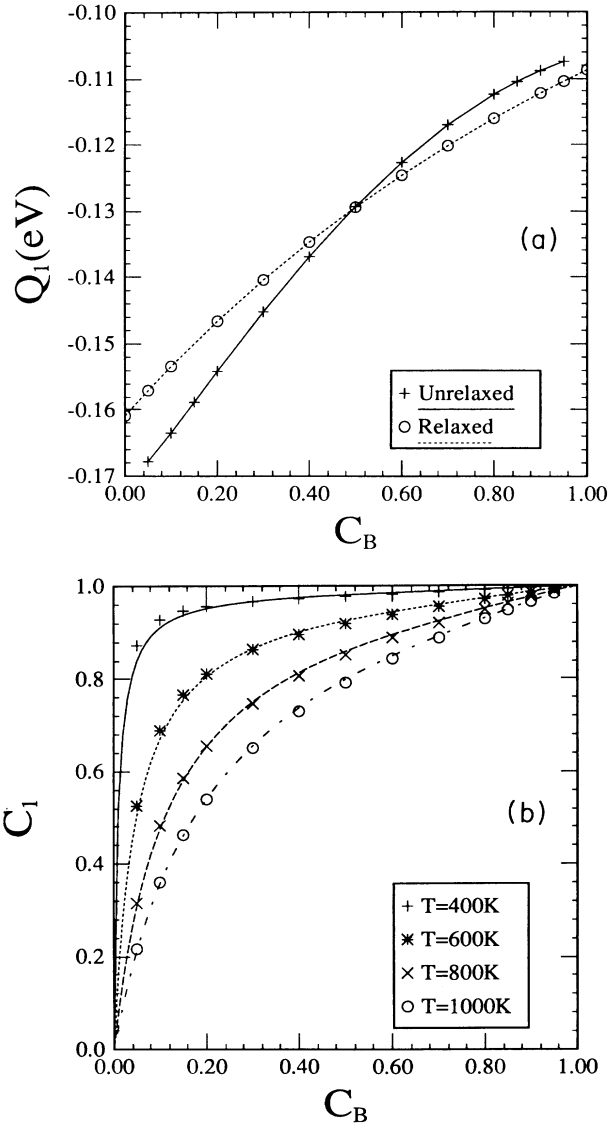

FIG. 11. (a) The heat of surface segregation Q_1 $(=\partial F/\partial C_1-\partial F/\partial C_B)$ for the relaxed surface (circle) and the unrelaxed surface (plus) vs the bulk concentration C_B. (b) The Cu concentration on the first-layer C_1 given by the simulation (symbols) and by a linear interpolation between the unrelaxed pure Ni and pure Cu Q_1 values (line) vs the bulk concentration C_B. The plus and solid line, asterisk and dotted line, cross and dashed line, and the circle and dashed-dotted line are for 400, 600, 800, and 1000 K, respectively.

to investigate surface-segregation and surface thermodynamic trends across a wide range of alloy compositions and temperatures.

Finally, we note that the data presented here represent the results of approximately 120 atomistic simulations in which the equilibrium composition profile and surface thermodynamics were determined. Since the focus of the current work was to determine *trends* in surface-segregation behavior, such a large number of simulations was necessary. The only practical method for performing simulations on the required scale is the free-energy minimization method used here. Competing methods, such as Monte Carlo simulations in the (reduced) grand canonical ensemble, require orders of magnitude more computer time to achieve similar results (i.e., equilibrium segregation profiles). In addition, we note that there is essentially no other practical method available to obtain the free energy of segregation, which played an important role in understanding the results. Therefore, although the free-energy simulation methods employed are, by nature, approximate, they represent the only viable method to study trends in segregation thermodynamics.

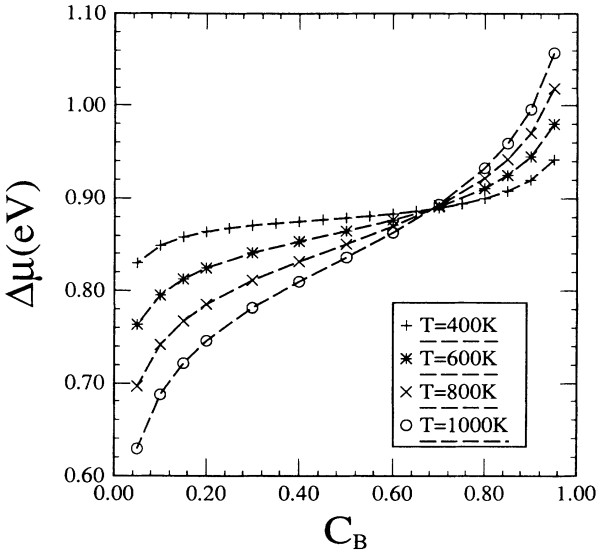

FIG. 13. The relationship between the Cu concentration and $\Delta\mu$.

V. CONCLUSIONS

Atomistic simulations of segregation to (100) free surface in Ni-Cu alloys have been performed for a wide range of temperatures and compositions within the solid solution region of the alloy phase diagram. In addition to the surface-segregation profile, surface structures, free energies, enthalpies, and entropies were determined. These simulations were performed within the framework of the free-energy simulation method, in which an approximate free-energy functional is minimized with respect to atomic coordinates and atomic-site occupation. For all alloy bulk compositions ($0.05 \leq C \leq 0.95$) and temperatures [$400 \leq T$ (K) ≤ 1000] examined, Cu segregates strongly to the surface and Ni segregates to the planes just below the surface. The width of the segregation profile is limited to approximately three atomic planes. The resultant segregation profiles are shown to be in good agreement with an empirical segregation theory. A simpler method for determining the equilibrium segregation in terms of the properties of unrelaxed pure Ni and pure Cu surface data is proposed and shown to be more accurate than existing empirical segregation analyses. The surface thermodynamic properties depend sensitively on the magnitude of the surface segregation. The enthalpy, entropy of segregation, and the change in the interlayer spacing ad-

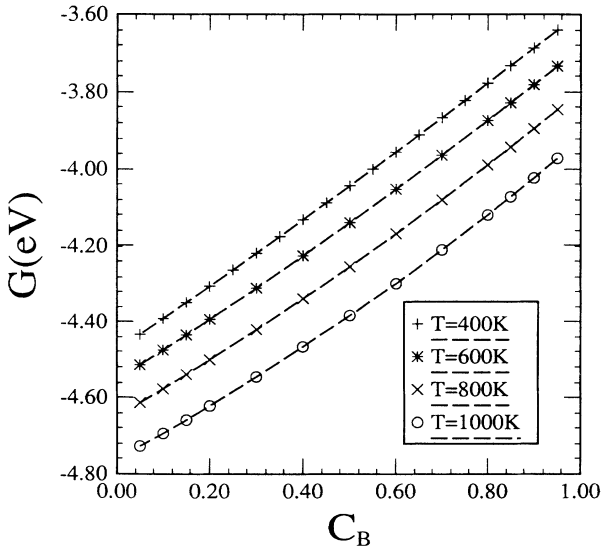

FIG. 12. The Gibbs free energy G as a function of Cu concentration at four different temperatures.

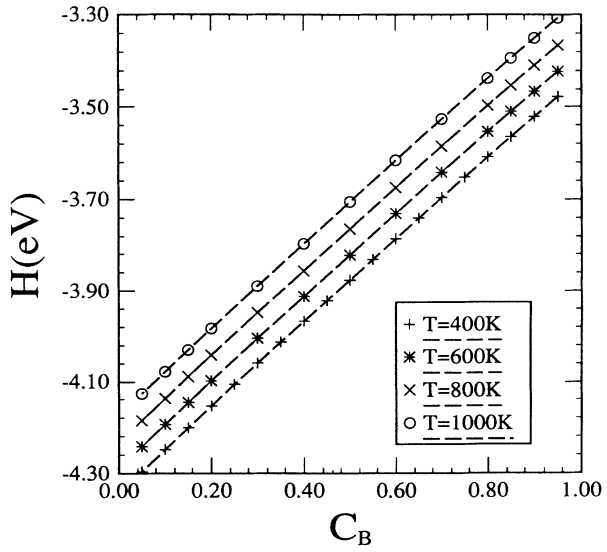

FIG. 14. The enthalpy H as a function of the bulk Cu concentration.

jacent to the surface are shown to vary linearly with the magnitude of the surface segregation.

ACKNOWLEDGMENTS

We gratefully acknowledge the Division of Materials Science of the Office of Basic Energy Sciences of the U. S. Department of Energy (DOE BES DMS), Grant No. FG02-88ER45367 for its support of this work. The work of R. L. was also supported, in part, by DOE BES DMS.

APPENDIX

Before the structure, segregation and properties of surfaces in Cu-Ni alloys can be examined, it is first necessary to determine the properties of perfect crystals in this alloy system. We determined the structure and properties of perfect solid-solution Cu-Ni crystals by minimizing the grand potential at fixed values of temperature, concentration, and pressure. In the present calculations, we set the external pressure to zero. The composition was fixed in terms of the chemical-potential difference between Ni and Cu atoms. Since the only crystalline structure that occurs in the Cu-Ni phase is the face-centered-cubic structure (above 250 K), the grand potential minimization was performed with respect to the single-lattice parameter.

The Gibbs free energy G is plotted as a function of Cu concentration at four different temperatures in Fig. 12. The free energy monotonically increases with increasing Cu concentration and decreasing temperature. Concentration is varied in these simulations by changing the chemical-potential difference $\Delta\mu = -\partial G/\partial C_B$. The relationship between concentration and $\Delta\mu$ is nonlinear, as shown in Fig. 13. The slopes of the curves in this plot increase with increasing temperature and become horizontal in the limit that T goes to zero due to the requisite zero solubility at zero temperature.

The enthalpy H is plotted as a function of bulk concentration in Fig. 14. H is equal to the total internal energy since the simulations were performed at zero pressure, and is equal to the potential energy plus $3k_BT$. The $3k_BT$ comes from the vibrational energy within the classical approximation. The enthalpy increases in a nearly linear manner as the concentration is increased from pure Ni to pure Cu. Increasing temperature simply shifts the enthalpy versus C_B curves to higher enthalpy.

The entropy consists of two parts: vibrational and configurational. The vibrational entropy S_v is plotted against the bulk concentrations C_B in Fig. 15(a). Like the enthalpy, the vibrational entropy increases with increas-

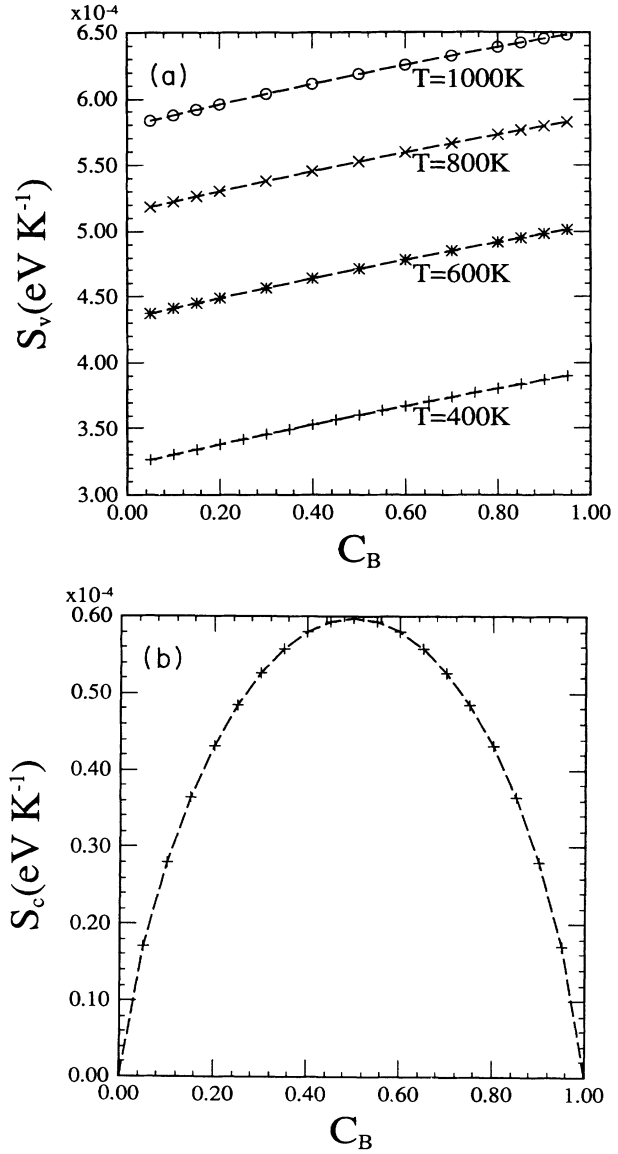

FIG. 15. (a) The vibrational entropy S_v vs the bulk concentration C_B. (b) Concentration dependence of the configurational entropy S_c.

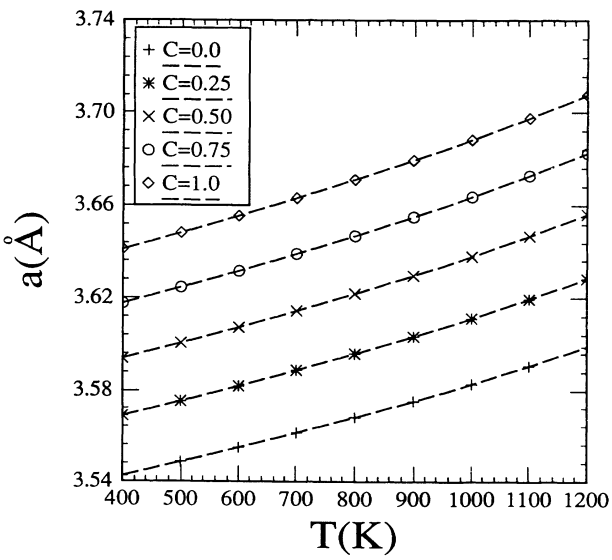

FIG. 16. The temperature dependence of the lattice parameter, for five different alloy compositions.

ing Cu concentration in a nearly linear manner and increasing temperature simply shifts these curves to higher entropy. The concentration dependence of the configurational entropy S_c is shown in Fig. 15(b). Within the simple point approximation employed within the present simulations, S_c is simply a function of concentration and is independent of atom type or temperature.

Although the free-energy model is harmonic in nature, the fact that the interatomic potentials are anharmonic result in a nonzero coefficient of thermal expansion. The temperature dependence of the lattice parameter is indicated in Fig. 16 for five different alloy compositions. These curves may be fitted with a second-order polynomial, yielding $a(T)=3.522+4.55\times10^{-5}T+1.54\times10^{-8}T^2$ for pure Ni and $a(T)=3.618+5.02\times10^{-5}T+2.05\times10^{-8}T^2$ for pure Cu where T is in kelvin and $a(T)$ is in angstroms. This leads to a room-temperature, linear-expansion coefficient of 1.5×10^{-5} for Ni and 1.7×10^{-5} for Cu, which in both cases is within 15% of the experimental values.

[1]P. Van der Plank and W. M. H. Sachtler, J. Catal. **12**, 35 (1968).

[2]J. H. Sinfelt, J. L. Carter, and D. J. C. Yates, J. Catal. **24**, 283 (1972).

[3]V. Ponec and W. M. H. Sachtler, J. Catal. **24**, 250 (1972).

[4]T. M. Buck, in *Chemistry and Physics of Solid Surfaces IV,* edited by R. Vanselow and R. Howe (Springer-Verlag, Berlin, 1982).

[5]A. Joshi, in *Interfacial Segregation,* edited by W. C. Johnson and J. M. Blakely (American Society for Metals, Metals Park, OH, 1979).

[6]P. R. Webber, C. E. Rojas, P. J. Dobson, and D. Chadwick, Surf. Sci. **105**, 20 (1981).

[7]K. Wandelt and C. R. Brundle, Phys. Rev. Lett. **46**, 1529 (1981).

[8]F. J. Kuijers and V. Ponec, Surf. Sci. **68**, 294 (1977).

[9]C. R. Helms and K. Y. Yu, J. Vac. Sci. Technol. **12**, 276 (1975).

[10]K. Watanabe, M. Hashiba, and T. Yamashina, Surf. Sci. **61**, 483 (1976).

[11]G. Ertl and J. Kuppers, Surf. Sci. **24**, 104 (1974).

[12]D. T. Quinto, V. S. Sundaram, and W. D. Robertson, Surf. Sci. **28**, 504 (1971).

[13]Y. Takasu and H. Shimizu, J. Catal. **29**, 479 (1973).

[14]C. R. Helms, J. Catal. **36**, 114 (1975).

[15]D. T. Ling, J. N. Miller, I. Lindau, W. E. Spicer, and P. M. Stefan, Surf. Sci. **74**, 612 (1978).

[16]P. J. Durhan, R. G. Jordan, G. S. Schal, and L. T. Wille, Phys. Rev. Lett. **53**, 2038 (1984).

[17]K. Wandelt and C. R. Brundle, Phys. Rev. Lett. **46**, 1529 (1981).

[18]D. G. Swartfager, S. B. Ziemecki, and M. J. Kelly, J. Vac. Sci. Technol. **19**, 185 (1981).

[19]H. H. Brongersma and T. M. Buck, Surf. Sci. **53**, 649 (1975).

[20]H. H. Brongersma, M. J. Sparnay, and T. M. Buck, Surf. Sci. **71**, 657 (1978).

[21]H. H. Brongersma, P. A. J. Ackermans, and A. D. van Langeveld, Phys. Rev. B **34**, 5974 (1986).

[22]Y. S. Ng, T. T. Tsong, and S. B. McLane, Jr., Phys. Rev. Lett. **42**, 588 (1979).

[23]Y. S. Ng, T. T. Tsong, and S. B. McLane, Jr., J. Appl. Phys. **51**, 6189 (1980).

[24]T. Sakurai, T. Hashizume, A. Jimbo, A. Sakai, and S. Hyodo, Phys. Rev. Lett. **55**, 514 (1985).

[25]T. Sakurai, T. Hashizume, A. Kobayashi, A. Sakai, S. Hyodo, Y. Kuk, and H. W. Pickering, Phys. Rev. B **34**, 8379 (1986).

[26]S. M. Foiles, Phys. Rev. B **32**, 7685 (1985).

[27]S. M. Foiles, Phys. Rev. B **40**, 11502 (1989).

[28]J. Eymery and J. C. Joud, Surf. Sci. **231**, 419 (1990).

[29]S. Mukherjee, J. L. Moran-Lopez, V. Kumar, and K. H. Bennemann, Phys. Rev. B **25**, 730 (1982).

[30]S. Mukherjee and J. L. Moran-Lopez, Prog. Surf. Sci. **25**, 139 (1987).

[31]S. Mukherjee and J. L. Moran-Lopez, Surf. Sci. **188**, L742 (1987).

[32]Y. C. Cheng, Phys. Rev. B **34**, 7400 (1986).

[33]H. F. Lin, C. L. Wang, and Y. C. Cheng, Solid State Commun. **59**, 253 (1986).

[34]F. L. Williams and D. Nason, Surf. Sci. **45**, 377 (1974).

[35]R. Najafabadi, H. Y. Wang, D. J. Srolovitz, and R. LeSar, Acta Metall. Mater. **39**, 3071 (1991); H. Y. Wang, R. Najafabadi, D. J. Srolovitz, and R. LeSar, in *Defects in Materials,* edited by Paul D. Bristowe, J. Ernest Epperson, J. E. Griffith, and Z. Lilietal-Weber, MRS Symposia Proceedings No. 209 (Materials Research Society, Pittsburgh, 1991).

[36]H. Y. Wang, R. Najafabadi, D. J. Srolovitz, and R. LeSar, Philos. Mag. (to be published).

[37]R. LeSar, R. Najafabadi, and D. J. Srolovitz, Phys. Rev. Lett. **63**, 624 (1989).

[38]R. LeSar, R. Najafabadi, and D. J. Srolovitz, J. Chem. Phys. **94**, 5090 (1991).

[39]M. S. Daw and M. I. Baskes, Phys. Rev. Lett. **50**, 1285 (1983); Phys. Rev. B **29**, 643 (1984).

[40]S. M. Foiles, M. I. Baskes, and M. S. Daw, Phys. Rev. B **33**, 7983 (1986).

[41]R. Najafabadi, D. J. Srolovitz, and R. LeSar, J. Mater. Res. **5**, 2663 (1990).

[42]R. Najafabadi, D. J. Srolovitz, and R. LeSar, J. Mater. Res. **6**, 999 (1991).

[43]K. Huang, *Statistical Mechanics* (Wiley, New York, 1963).

[44]A. P. Sutton and R. W. Balluffi, *Crystal Interfaces* (Oxford University Press, Oxford, to be published).

[45]R. H. Fowler and E. A. Guggenheim, *Statistical Thermodynamics* (Cambridge University Press, Cambridge, 1939).

[46]P. Wynblatt and R. C. Ku, in *Interfacial Segregation,* edited by W. C. Johnson and J. M. Blakely (American Society for Metals, Metals Park, OH, 1979), p. 115.

[47]R. S. Jones, Phys. Rev. B **41**, 3256 (1989).